Further Developments of Normal Mode Theory of Lee Cyclogenesis: Isentropic Coordinate Model

A. TREVISAN

CNR-FISBAT, Bologna, Italy

L. FERRANTI*

Department of Physics, Bologna, Italy

P. MALGUZZI

CNR-FISBAT, Bologna, Italy

(Manuscript received 30 December 1987, in final form 6 June 1988)

ABSTRACT

This work is an extension of the normal mode theory of lee cyclogenesis in that it removes all the simplifications and restrictive assumptions contained in previous formulations. Linearized primitive equations in isentropic coordinates are integrated in time to find the most unstable eigenmode. The appropriate boundary condition for such a model applied either at $z = 0$ or $z = h$ is derived. Results obtained in the β-plane with a realistically steep and high isolated topography are discussed in relation to the basic state characteristics. Limits and prospects with respect to theory verification are also discussed.

1. Introduction

Considerable advances in the description of real cases of cyclogenesis (Radinovich 1986; Pichler and Steinacker 1987) in the lee of the Alps, as well as in forecasting skill (Dell'Osso 1984) have been achieved in recent years. At the same time, some theories have been developed with the aim of explaining the observed phenomenology (Speranza et al. 1985; Pierrehumbert 1985; Smith 1984, 1986; Mattocks and Bleck 1986; for a review see Mesinger and Pierrehumbert 1986). Because of the contrast between the high degree of simplification involved in the various theories and the complexity of the phenomenon, verification is still at a very preliminary stage (Egger 1988). It is conceivable that significant effort is needed before this gap can be filled.

The theory originally formulated by Speranza et al. (1985), and subsequently developed by Buzzi and Speranza (1986) and Malguzzi et al. (1987; hereafter referred to as MTS) deals with orographically modified baroclinic waves. In the same sense that a midlatitude developing cyclone wave is described by the most unstable eigenfunction of the baroclinic instability problem, the development of a cyclone wave in the presence of a topographic obstacle can be described by the same instability problem with orography. The theory accounts for the orographic effect induced on a developing baroclinic wave and thus reproduces the difference field observed between mountain and no-mountain numerical integration experiments. The dipole structure (specifically a low to the south and high to the north of the barrier scaling on the Rossby deformation radius), observed in both idealized and real data simulations of lee cyclogenesis, stands out as the orographic effect which is captured under highly simplified conditions.

This work represents a further step in the development of this theory in that it removes all the simplifications which are not inherent in the formulation of the theory itself. Since a ridgelike mountain, like that used in MTS, is not representative of the Alps and quasi-geostrophic dynamics is not adequate to deal with high and steep mountains, we consider here a primitive equation model of baroclinic instability in the presence of an obstacle having realistic horizontal and vertical scales.

In section 2 the model is described, namely the linearized version of the isentropic, channel model already used in previous experiments on Alpine cyclogenesis (Trevisan 1976). In particular, the numerical discre-

* Present affiliation: ECMWF, Reading, England.

Corresponding author address: Dr. Anna Trevisan, Dinamica Atmospferia, FISBAT-CNR, c/o Dipartimento di Fisica, Via Irnerio, 46, I-40126 Bologna, Italy.

tization of the continuity equation applied at the lower boundary is derived in appendix B.

In section 3 the results obtained by MTS are recovered, removing the limiting assumptions of that model (quasi-Boussinesq approximation, rigid lid, constant vertical shear), and it is shown that the application of the lower boundary condition at $z = 0$, instead of $z = h$, does not significantly affect the results. This finding allows the extension to the case of a two-dimensional mountain.

In section 4 results obtained in the β-plane with an isolated topography, having realistic horizontal and vertical scales for the Alps, are shown and the relationship with the basic state characteristics are discussed.

Finally, in section 5 conclusions are drawn, especially in relation to the problem of theory verification.

2. The model

In a previous paper (MTS) the eigenvalues and corresponding eigenvectors of the linear problem around a basic zonal wind were found by solving the characteristic equation. This procedure becomes impracticable when dealing with isolated mountains due to the dimension of the linear problem. One possible way of dealing with this problem consists in integrating in time numerically the equations of motion linearized around a basic state which is a solution of the nonlinear equations. In fact, an arbitrary initial condition will converge, after a sufficiently long time, to the most unstable eigenmode. In practice, the state of the system, $\vec{X}$, has to be renormalized after some (fixed) integration time interval T to avoid possible numerical overflow: the growth rate is thus computed as

$$\sigma = (1/T)\log(\|\vec{X}(t+T)\|/\|\vec{X}(t)\|) \tag{1}$$

once convergence is achieved.

A linearized version of the primitive equations model in isentropic coordinates is used (Eliassen and Raustein 1968; Bleck 1974; Trevisan 1976). The basic state is a zonal wind with *zero wind speed at the ground* and vertical and meridional shear in a periodic β-plane channel of dimension $L_x \times L_y$. Eliassen's staggered grid is used, combined with a leapfrog time integration scheme (time step of 2.5 min). Horizontal resolution is 100 km (distance between points of definition of the same variables). In the vertical we use 12 isentropic levels plus the ground surface. A variable L_x is used in order to allow for different perturbation wavelengths.

In order for the basic state to be a solution of the nonlinear equations when dealing with an isolated mountain $h(x, y)$, the lower boundary condition is applied at $z = 0$. However, the problem with topography in the form of an infinite ridge $h(y)$ can be approached without this assumption: in the following we will specify whether the boundary condition is applied at $z = 0$ or $z = h(y)$. The basic state is defined as in Eliassen and Raustein (1970). (A definition of the symbols and their numerical values is given in appendix A.) In the troposphere:

$$\bar{\pi} = c_p - k_T(\theta - \theta_s), \quad \theta_s < \theta < \theta_{TR} \tag{2a}$$

where

$$\theta_s = \theta_0 + \Delta\theta \tanh(y/y_0) \tag{2b}$$

is the potential temperature at $z = 0$ and, in the stratosphere:

$$\bar{\pi} = \pi_{TOP} + \frac{\pi_{TR} - \pi_{TOP}}{\theta_{TOP} - \theta_{TR}}(\theta_{TOP} - \theta) \quad \theta_{TR} \leqslant \theta \leqslant \theta_{TOP} \tag{3}$$

where θ_{TOP} and π_{TOP} are, respectively, the basic state potential temperature and Exner function at the top of the model atmosphere (the uppermost isentropic surface, $\theta = \theta_{TOP} = 400$ K, is a free surface at constant pressure $P = 100$ mb) and where θ_{TR} and π_{TR} are the same quantities computed at the tropopause which is defined as

$$\pi_{TR}(y) = \begin{cases} \pi_{TOP} + C(\theta_C - \theta_{TR}(y)) & \text{(4a)} \\ c_p - k_T(\theta_{TR}(y) - \theta_s(y)) & \text{(4b)} \end{cases}$$

Equation (4b) guarantees the continuity of $\bar{\pi}(y, z)$ at $\theta = \theta_{TR}$. This basic wind consists of a midlatitude jet with maximum wind speed at the tropopause: for a schematic description of its vertical profile see Eliassen (1970). The choice of a $\tanh(y)$ temperature profile gives a symmetric wind profile in the troposphere centered at $y = 0$ with half width y_0.

The linearized primitive equations in isentropic coordinates read

$$u'_t + \bar{U}u'_x + v'\bar{U}_y - fv' = -M'_x \tag{5a}$$

$$v'_t + \bar{U}v'_x + fu' = -M'_y \tag{5b}$$

$$p'_{t\theta} = -(\bar{U}p'_\theta + u'\bar{P}_\theta)_x - (v'\bar{P}_\theta)_y \tag{5c}$$

$$M'_\theta = R(\bar{P}/P_0)^{(R-c_p)/c_p}p'/P_0 \tag{5d}$$

Additional equations at the ground $z = h(x, y)$ are given by

$$u'_t + \bar{U}u'_x + v'\bar{U}_y - fv' + R\bar{\theta}[(\bar{P}/P_0)^{(R-c_p)/c_p}p']_x/P_0 = 0 \tag{6a}$$

$$v'_t + \bar{U}v'_x + fu' + c_p\theta'(\bar{P}/P_0)^{R/c_p} + \bar{\theta}R[(\bar{P}/P_0)^{(R-c_p)/c_p}p']_y/P_0 = 0 \tag{6b}$$

$$p'_{t\theta} + (\bar{U}p'_\theta + u'\bar{P}_\theta)_x + (v'\bar{P}_\theta)_y = 0 \tag{6c}$$

$$\theta'_t + \bar{U}\theta'_x + v'\bar{\theta}_y = 0 \tag{6d}$$

where $\bar{\theta}(x, y)$ is the basic state potential temperature at $z = h(x, y)$. Note that $g\vec{\nabla}h(x, y)$ does not appear in (6a) and (6b) because such a term, being independent of the prognostic variables, enters only the basic state balance. When the lower boundary condition is applied at $z = 0$, Eqs. (6a–d) become

$$u'_t - fv' + R\bar{\theta}[(\bar{P}/P_0)^{(R-c_p)/c_p}p']_x/P_0 = g\bar{\theta}_y w'/(f\bar{\theta}) \quad (7a)$$

$$v'_t + fu' + c_p\theta'(\bar{P}/P_0)^{R/c_p} + \bar{\theta}R[(\bar{P}/P_0)^{(R-c_p)/c_p}p']_y/P_0 = 0 \quad (7b)$$

$$p'_{t\theta} + (u'\bar{P}_\theta)_x + (v'\bar{P}_\theta)_y = gP_0{}^{R/c_p}w'/(R\bar{\theta}\bar{P}^{(R-c_p)/c_p}) \quad (7c)$$

$$\theta'_t + v'\bar{\theta}_y = -gw'/(k_T\bar{\theta}), \quad \bar{\theta} = \theta_s \quad (7d)$$

where

$$w' = u'h_x + v'h_y.$$

Terms on the right-hand sides of (7a) and (7d) represent the vertical advection of the basic state zonal velocity and potential temperature at $z = 0$, respectively. The term on the right-hand side of (7c) represents the mass input associated with the vertical motion at $z = 0$ and is derived in appendix B. Equations (7) are linearized around the basic state defined above.

3. Results with an infinite ridge in the f-plane

The purpose of this section is twofold. First, we wish to recover previous results (MTS), since the present formulation does not suffer from the simplifications introduced in MTS. In fact, the main differences consist in the following:

(a) The quasi-Boussinesq approximation is removed here.

(b) The basic state wind profile is more realistic; in particular, it contains a tropopause and a varying stratification and vertical shear.

(c) The upper boundary condition is a free surface.

(d) β-effect can be included, although β is set equal to zero in this section for direct comparison.

Furthermore, it is desirable to verify whether the application of the lower boundary condition at $z = 0$ does not affect the results significantly, as was the case in MTS. This is an important step since, as already mentioned, the case of two-dimensional topography $h(x, y)$ can only be dealt with if the lower boundary condition is applied at $z = 0$, in which case the basic state with zero wind at $z = 0$ is a stationary solution. Figure 1 shows the most unstable eigenmodes obtained without a mountain (Fig. 1a), with the lower boundary condition applied at $z = h(y)$ (Fig. 1b) and at $z = 0$ (Fig. 1c). The topography is the same as in MTS, namely an infinite ridge with triangular section of 150 km half-width at the base and 2000 m height. Other parameters are $L_x = 5000$ km, $L_y = 5000$ km, $\Delta\theta = 19$ K, and $y_0 = 1320$ km. The "bulk" Richardson number can be estimated by applying the thermal wind relationship

$$U_z = -\frac{g}{f_0}\frac{\theta_y}{\theta} \quad (8)$$

to the temperature gradient given by (2b) and by averaging the vertical wind shear over a region having a width of $2y_0$. The result is

$$\mathrm{Ri} = \frac{N^2}{\left(\frac{1}{2y_0}\int_{-y_0}^{y_0} U_z dy\right)^2} \approx \frac{f_0{}^2 y_0{}^2}{k_T(\Delta\theta)^2(\tanh^2 1)}$$

where the Brünt–Väisälä frequency N^2 has been estimated, using the form of the hydrostatic equation $g\frac{\partial z}{\partial \pi} = -\theta$ and (2a), as

$$N^2 = \frac{g}{\theta}\frac{\partial\theta}{\partial z} = \frac{g^2}{\theta^2}\frac{1}{k_T}.$$

By setting $k_T = 8$, we get $N^2 = 1.4 \times 10^{-4}\ \mathrm{s}^{-2}$ and Ri = 10, which is the value used in MTS. The e-folding time estimated from (1) for the eigenmode shown in Fig. 1b is about 2 days. As can be readily seen, the basic asymmetry introduced by the mountain is in agreement with the findings of MTS. In particular, the approximation introduced in the boundary condition performs satisfactorily for our purposes.

4. Results with isolated topography

The scope of the present section is to generalize previous results (Speranza et al. 1985; Buzzi and Speranza 1986; MTS) in the case of a steep mountain of limited east–west extension. An elongated mountain centered in and parallel to the baroclinic flow is considered, in order to reproduce the symmetry invoked by the normal mode theory of Alpine cyclogenesis, i.e., enhancement of the perturbation to the south and weakening to the north of the barrier. In particular, we consider the "rooflike" mountain shown in Fig. 2 obtained by truncating the ridge used in the previous section.

Investigation of the symmetry characteristics of the most unstable normal mode in relation to the basic state parameters and domain geometry shows that the symmetry (referring specifically to the feature just described) is basically determined by the phase speed of the normal mode itself. In turn, the phase speed depends essentially on the wind speed of the basic state zonal wind averaged in the region affected by the perturbation growth.

In essence, slowly moving baroclinic waves tend to be confined south of the mountain showing a symmetry similar to the case of the infinite ridge, the only difference being that the modification is substantially restricted to the part of the domain near the mountain. The fact that the topographic modification is stronger when the phase speed is weaker is known from observation of real cases of lee cyclogenesis (see, for a discussion, Tosi et al. 1983).

The dependence on the basic state wind speed was not as critical, when dealing with the infinite ridge, as

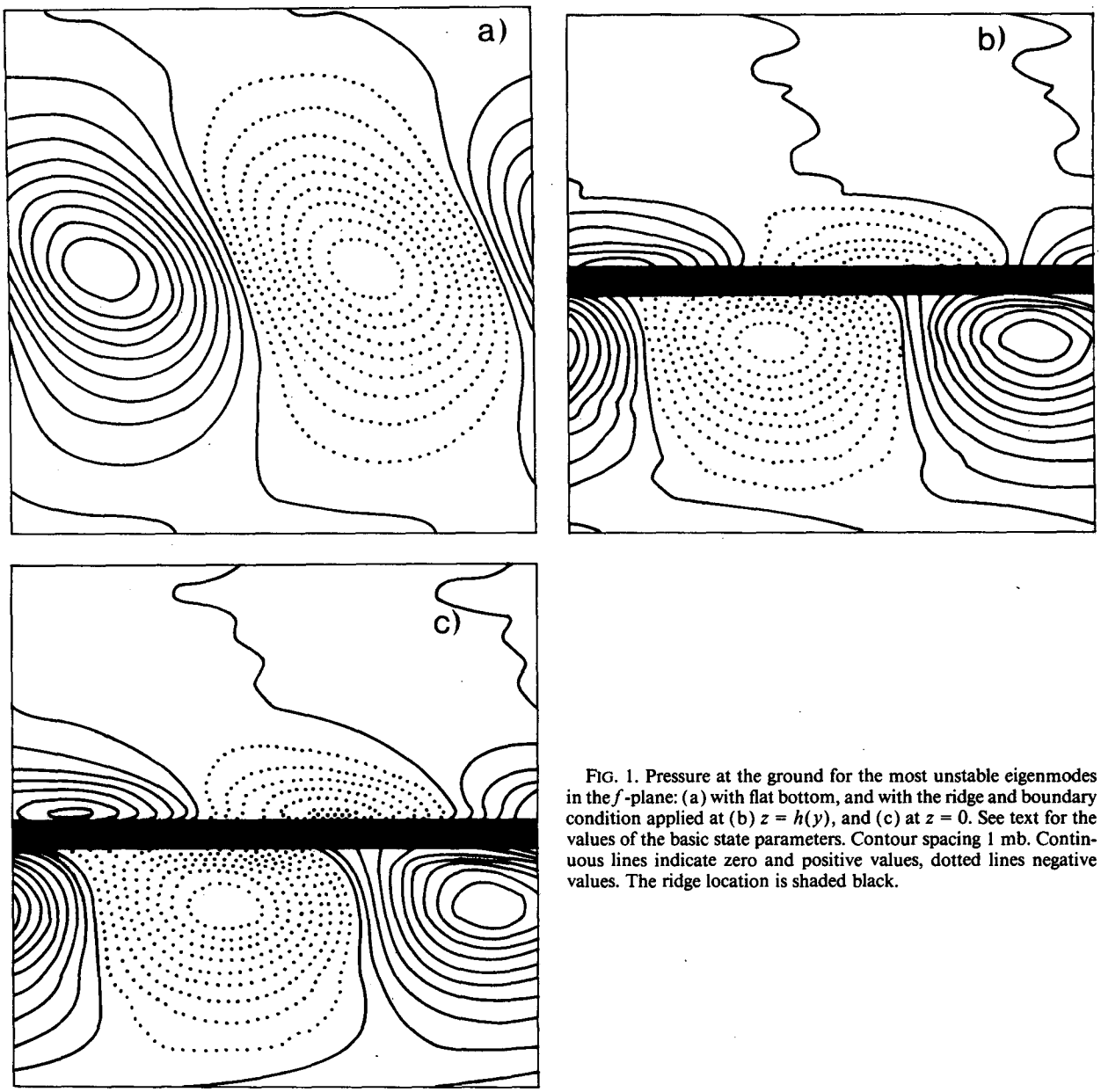

FIG. 1. Pressure at the ground for the most unstable eigenmodes in the f-plane: (a) with flat bottom, and with the ridge and boundary condition applied at (b) $z = h(y)$, and (c) at $z = 0$. See text for the values of the basic state parameters. Contour spacing 1 mb. Continuous lines indicate zero and positive values, dotted lines negative values. The ridge location is shaded black.

it is here; it is found that, in order to obtain the required symmetry also with an isolated mountain, it is necessary to modify the basic state parameters used in section 3. This can be done in two ways: the average wind speed of the basic state in the central region can be reduced by increasing y_0 [see Eq. (2b) and (8)]. Alternatively, it can be reduced by decreasing the equator-to-pole temperature difference (parameter $\Delta\theta$) while leaving the meridional scale of the jet unchanged. Provided the average momentum in the region of interest is the same, these two procedures are equivalent.

We have studied the following range of parameters: $\Delta\theta = 19 \pm 6$ K, $y_0 = 2000 \pm 1000$ km, and $L_x = 5000 \pm 1000$ km, by varying the value of one parameter at

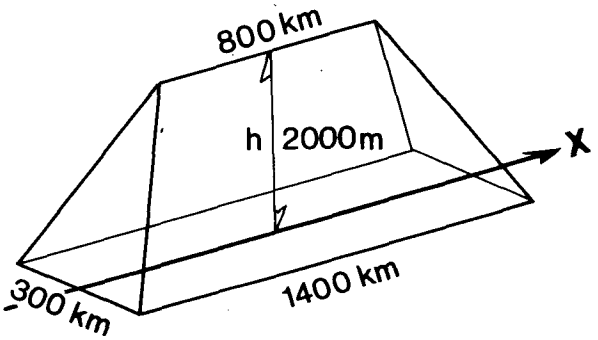

FIG. 2. Schematic representation of isolated topography; horizontal and vertical dimensions are indicated.

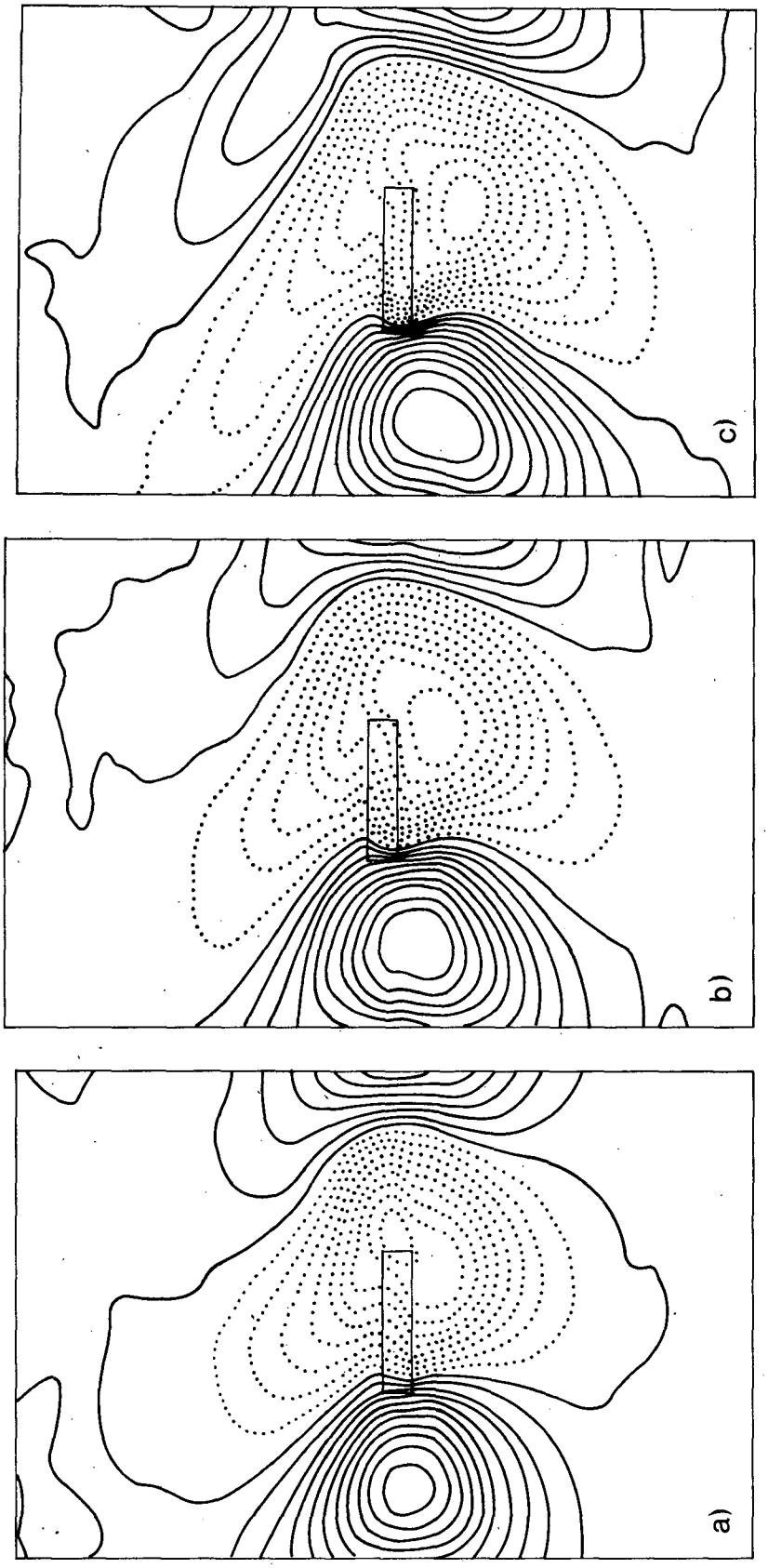

FIG. 3. Pressure at $z = 0$ for the most unstable eigenmodes in the β-plane with the isolated topography of Fig. 2, obtained for different values of the jet half-width: (a) $y_0 = 1320$, (b) 2000 and (c) 3000 km. Other parameter values are $\Delta\theta = 19$ K, $L_y = 7500$ km, and $L_x = 5000$ km. Resulting phase speeds and e-folding times are 10.5, 7.0, and 4.5 m s^{-1} and 1.5, 2, and 3 days, respectively. Isoline contours as in Fig. 1.

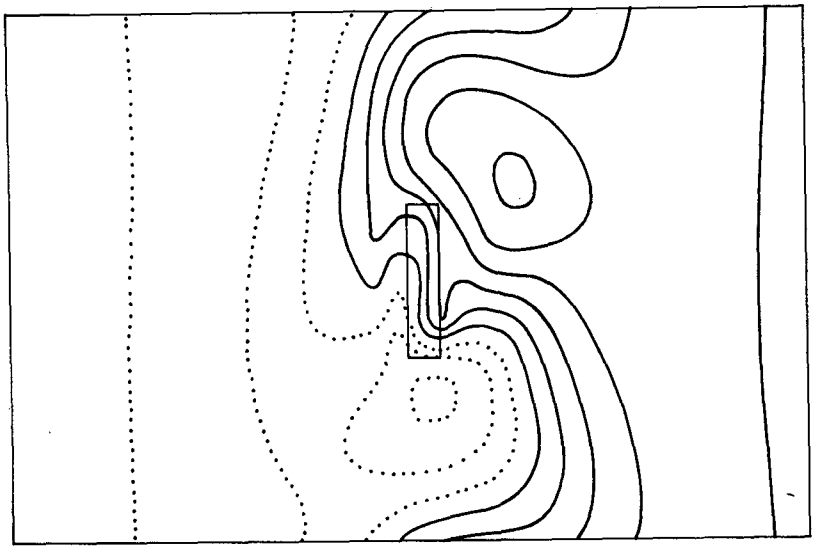

FIG. 5. Total potential temperature (basic state plus perturbation temperature with twice the normalized amplitude used in Figs. 3 and 4) at $z = 0$ for the eigenmode of Fig. 3b. Contour spacing 5 K.

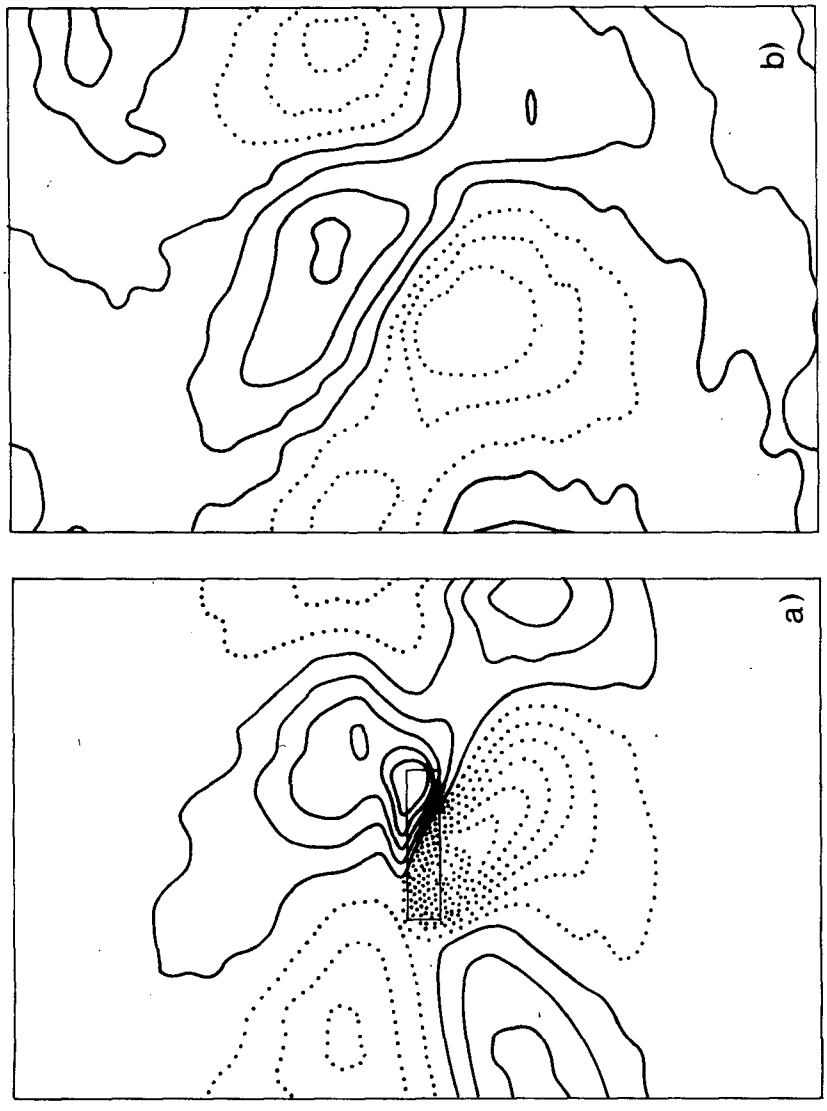

FIG. 4. Difference fields between the eigenmode shown in Fig. 3b and corresponding no-mountain normal mode. Pressure at (a) $z = 0$ with contour spacing 0.5 mb, and geopotential height at (b) 500 mb with contour spacing 250 $m^2 s^{-2}$. Continuous lines indicate zero and positive values, and dotted lines negative values.

a time. The asymmetry of the mode is more pronounced when y_0 is largest or $\Delta\theta$ is smallest, i.e., in cases for which the perturbation phase speed is smallest. The asymmetry is, in turn, lost in the opposite cases ($y_0 \leqslant 1300$ km, $\Delta\theta \geqslant 24$ K). The phase speed weakly depends also on the wavelength and, again, the asymmetry is more pronounced for $L_x = 6000$ km (phase speed 6 m s^{-1}) than for $L_x = 4000$ km (phase speed 8 m s^{-1}).

The change of asymmetry with phase speed is well illustrated in Figs. 3a–c which show the most unstable normal modes at $z = 0$ obtained in the β-plane, with $\Delta\theta = 19$ K and $y_0 = 1320$, 2000, and 3000 km, respectively. The phase speed is 10.5, 7, and 4.5 m s^{-1} in the three cases, respectively.

Figure 4 shows the difference fields between mountain and no-mountain experiments at $z = 0$ and 500 mb for the intermediate case shown in Fig. 3b, and computed at the time shown in the figure (a time when the cyclone is well developed in the lee of the topography). The dipole structure, found in previous studies, is reproduced, but the orographic modification is somewhat weaker here than in real cases at 500 mb. (The arbitrary perturbation amplitude is chosen to give a 10 mb pressure low at $z = 0$). Another interesting feature of the difference field is the dipole orientation, which presents a northeast, southwest tilt of about 30°. This is also a characteristic observed in real cases (see Fig. 2 of Speranza et al. 1985).

The total temperature field (perturbation and basic state) at $z = 0$, for the case shown in Fig. 3b, shows a realistic frontal deformation (Fig. 5) across the mountain.

Starting from an arbitrary initial perturbation, the time scale expected for the most unstable normal mode to emerge depends on the growth rate of all other modes. With an isolated mountain of small volume (compared to the total domain volume), the eigenvalues are the same as for the flat bottom case. The difference in growth rate between the first and second most unstable modes, already quite substantial with uniform wind, is further augmented in the presence of lateral shear (see, for example, Fig. 2 of MTS in the flat bottom case $h = 0$). Thus, our study is limited to the most unstable mode.

Beyond these general considerations, we mention one specific example in which this time scale has been evaluated. We have integrated the linear equations starting from an initial perturbation in the form of a meridionally symmetric, zonally wavelike disturbance with the associated cyclone positioned 2500 km upstream of the mountain (basic state parameters as in Fig. 3b). After about 4 days, when the cyclone reaches the mountain, the perturbation has already settled into the asymmetric modal structure observed in Fig. 3b. Note that this time scale is shorter than one wave period, so that an initially symmetric transient is able to converge to the asymmetric structure without having to recycle through the channel.

5. Conclusions

The goal of this paper is to extend the normal mode theory of lee cyclogenesis to the most general case, i.e., to remove all the restrictive hypotheses introduced in previous works except, of course, the hypothesis that the time evolution we are interested in can be approximated in terms of the most unstable normal mode of a zonal basic state; in fact, this characterizes the theory itself. In a variety of cases studied, in a realistic range of parameter space, the most unstable normal mode in the presence of high and steep localized topography exhibits the typical configuration expected for lee cyclogenesis.

In principle, the theory can be verified, through comparison with nonlinear numerical simulations which faithfully reproduce the time development of the lee cyclone (Egger 1988), by showing that the approximations implied by the theory are not essential to the physical mechanisms involved. As far as linearity is concerned, there are cases in which, at least for a short time span, a basic state and a perturbation can be somehow identified in real evolutions. An example is given by the cyclonic development on the western side of the Rocky Mountains reported by Buzzi et al. (1987): a pressure perturbation of weak amplitude develops over a flow initially parallel to the mountain chain (see Fig. 1 of Buzzi et al. 1987). Thus, in this case the verification of the theory seems to be straightforward.

The case of the Alps is not so clear cut because deep lee cyclogenesis is often associated with finite amplitude baroclinic waves and frontal structures impinging over the mountain. The role played by the amplitude of the incoming wave cannot be understood invoking the normal mode theory alone. We suggest a possible procedure that can be adopted in verification: starting from a successful numerical experiment, which contains a large amplitude baroclinic wave at the time of interaction with the mountain, one could define a "mean" zonal basic state and find the most unstable normal mode for that basic state. (One should be aware of the arbitrariness of this definition.) This procedure also implies the approximation of a particular nonlinear evolution with the linear amplification of our orographically modified normal mode. In particular, given the importance of the phase speed in determining the symmetry of the most unstable normal mode, verification of the theory must take the results of this work into account when choosing the appropriate basic state and geometry. For example, the role played by the wave amplitude may simply be that of implying a smaller phase speed and, thus, a longer interaction time with the mountain. If this is the case, such effect must be

somehow included through a proper definition of the zonal basic state.

Acknowledgments. The authors wish to thank J. Egger, I. M. Held and the anonymous reviewer for helpful comments.

The computer time needed to complete this work has been made available by the Program for the Use of Large Vector Computers of the CINECA (Centro di Calcolo Inter-universitario dell'Italia Nord-Orientale) of Bologna.

APPENDIX A

List of Symbols

L_x, L_y	zonal and meridional width of the domain
h	topography
x, y, θ	zonal, meridional, and vertical coordinate
$\theta = T(P_0/p)^{R/c_p}$	potential temperature
$\pi = c_p(p/P_0)^{R/c_p}$	Exner function
T	temperature
ρ	density
p	pressure
P_0	reference pressure [=1000 mb]
R	gas constant of dry air [=287 J K^{-1} kg^{-1}]
c_p	specific heat of dry air at constant pressure [=1004 J K^{-1} kg^{-1}]
$\bar{P}$	basic state pressure
$\bar{U}$	basic state velocity
$\bar{\pi}$	basic state Exner function
$\bar{\theta}$	basic state potential temperature at the ground
θ_s	basic state potential temperature at $z = 0$ [$\theta_s = \Delta\theta \tanh(y/y_0) + \theta_0$]
θ_0	average potential temperature at $z = 0$ (287 K)
y_0	jet half-width
$\Delta\theta$	half equator-to-pole temperature contrast
θ_{TOP}	potential temperature at upper boundary (400 K)
π_{TOP}	Exner function at upper boundary; $c_p(100/P_0)^{R/c_p}$ J K^{-1} Kg^{-1}
θ_{TR}	potential temperature at tropopause level
π_{TR}	Exner function at tropopause level
$k_T = -\dfrac{\partial\bar{\pi}}{\partial\theta}$	= 8 m^2 s^{-2} K^{-2}
$C = \dfrac{\partial\pi_{TR}}{\partial\theta_{TR}}$	= 2.81 m^2 s^{-2} K^{-2}
θ_C	= 365 K
u', v', w'	perturbation zonal, meridional and vertical velocity
p'	perturbation pressure
M'	perturbation Montgomery streamfunction
g	gravity constant [=9.8 m s^{-2}]
f	Coriolis parameter
f_0	Coriolis parameter at 45° latitude
β	meridional gradient of Coriolis parameter at 45°
Ri	Richardson number
N^2	Brünt–Väisälä frequency

APPENDIX B

Continuity Equation at the Lower Boundary

We derive the form of the continuity equation to be used at the lower boundary in an isentropic model, both in the general case and when the topographic effect is considered at $z = 0$. Although explicit reference is made to isentropic coordinates note that the following formulas are applicable between any two material surfaces.

The mass conservation can be written, making use of the hydrostatic relationship, as

$$\begin{aligned} D/Dt(\rho dxdydz) &= -g^{-1}D/Dt(dxdydp) \\ &= -g^{-1}dpD/Dt(dxdy) - g^{-1}dxdyD/Dt(dp) \\ &= 0 \end{aligned} \tag{B1}$$

where

$$D/Dt = \partial_t|_q + u\partial_x|_q + v\partial_y|_q + (ds/dt)\partial_q$$

is the total derivative in the coordinate system (x, y, s), and where the small volume, $dxdydp$, is bounded above by a θ-coordinate surface and below by the ground, marked respectively by $q = \theta$ and $q = s$. The last term in (B1) can be expressed as

$$\begin{aligned} D/Dt(dp) &= D/Dt(p_\theta - p_s) \\ &= \partial_t p|_\theta + u\partial_x p|_\theta + v\partial_y p|_\theta \\ &\quad - (\partial_t p|_s + u\partial_x p|_s + v\partial_y p|_s) - w_s\partial_z p_s \\ &\approx \partial_t dp + \bar{u}\partial_x dp + \bar{v}\partial_y dp + w_s g\rho_s \end{aligned} \tag{B2}$$

where

$$\bar{u} = \frac{1}{2}(u_\theta + u_s), \quad \bar{v} = \frac{1}{2}(v_\theta + v_s)$$

and where the last term in (B2) is not present if the ground is a "true" material surface but is only present when the boundary condition is applied at $z = 0$ instead of $z = h$, due to the topographic effect. By combining (B1) and (B2) we finally get the evolution equation for $dp(x, y, t)$:

$$\begin{aligned} &\partial_t(dp) + \partial_x(\bar{u}dp) + \partial_y(\bar{v}dp) \\ &\qquad = gP_0{}^{R/c_p}w_s/(R\theta_s p_s{}^{(R-c_p)/c_p}) \end{aligned} \tag{B3}$$

where $w_s = u_s h_x + v_s h_y$ and the perfect gas law has

been applied. The linearized version of (B3) is the mass flux inside the volume $dx\ dy\ d\theta$ due to the vertical motion at $z = 0$, forced by the orography.

REFERENCES

Bleck, R., 1974: Short range prediction in isentropic coordinates with filtered and unfiltered numerical models. *Mon. Wea. Rev.*, **102,** 813–829.

Buzzi, A., and A. Speranza, 1986: A theory of deep cyclogenesis in the lee of the Alps. Part II: Effects of finite topographic slope and height. *J. Atmos. Sci.*, **43,** 2826–2837.

——, ——, S. Tibaldi and E. Tosi, 1987: A unified theory of orographic influences upon cyclogenesis. *Meteor. Atmos. Phys.*, **36,** 91–108.

Dell'Osso, L., 1984: High-resolution experiments with the ECMWF model: A case study. *Mon. Wea. Rev.*, **112,** 1853–1883.

Egger, J., 1988: Alpine lee cyclogenesis: Verification of theories. *J. Atmos. Sci.*, **45,** 2187–2203.

Eliassen, A., and E. Raustein, 1968: A numerical integration experiment with a model atmosphere based on isentropic coordinates. *Meteor. Ann.*, **5,** 45–63.

——, and ——, 1970: A numerical integration experiment with a six-level atmospheric model with isentropic information surfaces. *Meteor. Ann.*, **5,** 429–449.

Malguzzi, P., A. Trevisan and A. Speranza, 1987: Effects of finite height topography on nongeostrophic baroclinic instability: Implications to theories of lee cyclogenesis. *J. Atmos. Sci.*, **44,** 1475–1482.

Mattocks, C., and R. Bleck, 1986: Jet streak dynamics and geostrophic adjustment processes during the initial stages of lee cyclogenesis. *Mon. Wea. Rev.*, **114,** 2033–2056.

Mesinger, F., and R. Pierrehumbert, 1986: Alpine lee cyclogenesis: Numerical simulation and theory. *Scientific Results of the Alpine Experiment,* Vol. I. GARP-Publ., Ser. 27, 141–165.

Pichler, H., and R. Steinacker, 1987: On the synoptics and dynamics of orographically induced cyclones in the Mediterranean. *Meteor. Atmos. Phys.*, **36,** 108–117.

Pierrehumbert, R., 1985: A theoretical model of orographically modified cyclogenesis. *J. Atmos. Sci.*, **42,** 1244–1258.

Radinovich, D., 1986: On the development of orographic cyclones. *Quart. J. Roy. Meteor. Soc.*, **112,** 927–951.

Smith, R. B., 1984: A theory of lee cyclogenesis. *J. Atmos. Sci.*, **41,** 1159–1168.

——, 1986: Further development of a theory of lee cyclogenesis. *J. Atmos. Sci.*, **43,** 1582–1602.

Speranza, A., A. Buzzi, A. Trevisan and P. Malguzzi, 1985: A theory of deep cyclogenesis in the lee of the Alps. Part I: Modification of baroclinic instability by localized topography. *J. Atmos. Sci.*, **42,** 1521–1535.

Tosi, E., M. Fantini and A. Trevisan, 1983: Numerical experiments on orographic cyclogenesis: Relationship between the development of the lee cyclone and the basic flow characteristics. *Mon. Wea. Rev.*, **111,** 799–814.

Trevisan, A., 1976: Numerical experiments on the influence of orography on cyclone formation with an isentropic primitive equation model. *J. Atmos. Sci.*, **33,** 768–780.